Physics of the Earth and Planetary Interiors 301 (2020) 106452

Contents lists available at ScienceDirect

Physics of the Earth and Planetary Interiors

journal homepage: www.elsevier.com/locate/pepi

Lateral variation of the mantle transition zone beneath the Tibetan Plateau: Insight into thermal processes during Indian–Asian collision

Mijian Xu*, Zhouchuan Huang*, Liangshu Wang*, Mingjie Xu, Ning Mi, Dayong Yu

School of Earth Sciences and Engineering, Nanjing University, Nanjing 210023, China

ARTICLE INFO

Keywords:
Tibetan plateau
Receiver function
Mantle transition zone
Indian subduction
Volcanism

ABSTRACT

The Indian plate began to subduct under the Eurasian plate in the late Mesozoic. Since the Eocene, continuous continental collision has resulted in the uplift of the Tibetan Plateau with extensive volcanic activities. Geophysical and geochemical studies have suggested that the Indian plate subducted and that volcanism originated in the deep upper mantle. However, the depth range of the subduction and volcanism and the relationship between them are still unclear. Here, to image the mantle transition zone (MTZ) structures, we deployed new seismic stations and collected as much seismic data as possible from the Tibetan Plateau. We then calculated the receiver functions and analyzed them using the common conversion point stacking method. We found that the MTZ is thickened by ~20 km under the Lhasa block, where high-velocity anomalies are obvious in the MTZ. Apparent thinning of the MTZ by ~20 km was revealed under the Qiangtang and Songpan-Ganze blocks, confirming a component of depleted mid-oceanic ridge basalt in the magmatic rocks. Our results suggest that the Indian Plate has at least subducted to the MTZ, which has further induced mantle upwelling and volcanism in the Tibetan Plateau.

1. Introduction

The 410 km and 660 km discontinuities (hereafter referred to as the d410 and d660) of the upper and lower boundaries of the mantle transition zone (MTZ) are significant mineral phase transition interfaces. The transition from olivine to wadsleyite results in the d410, representing an exothermic process with a positive Clapeyron slope; the transition from ringwoodite to bridgmanite forms the d660, representing an endothermic process with a negative Clapeyron slope. A thinning MTZ with a depressed d410 and uplifted d660 is formed in hot environments (e.g., a mantle plume through the MTZ); thickening with an uplifted d410 and depressed d660 is formed in cold environments (e.g., a cold slab subducting into the lower mantle) (Bina and Helffrich, 1994).

The Tibetan Plateau was generally formed by collisions between the Lhasa, Qiangtang, Songpan-Ganze, and North China blocks from the Triassic to the Jurassic (Fig. 1) (Burtman and Molnar, 1993; Frederick et al., 1988; Gaetani et al., 1993; Yin and Harrison, 2000). The Indian plate has been subducted beneath the Eurasian plate since the Cretaceous to form the Himalayas (e.g., Brookfield, 1993; Burchfiel et al., 1992; England and Houseman, 1986; Replumaz et al., 2016; Royden et al., 2008; Yin and Harrison, 2000). Because of continental collision from the Eocene onward, oblique subduction of the Indian plate northward has led to continuous uplift of the Tibetan Plateau (e.g., Molnar and Tapponnier, 1975; Royden et al., 2008; Tapponnier et al., 2001; Yin, 2010; Yin and Harrison, 2000). Seismic observations have provided evidence for the tectonic evolution of the region. Teleseismic tomographic studies indicated the presence in the upper mantle of both subducted oceanic Indian lithosphere (with reversed motion indicated by high velocity anomalies) and continental lithosphere down to a depth of 200-km and beyond (Chen et al., 2017; Lei and Zhao, 2016; Li et al., 2008; Liang et al., 2012, 2016; Nunn et al., 2014; Replumaz et al., 2013; Wang et al., 2019; Zhang et al., 2012, 2015). In particular, some of these studies have shown high velocity bodies in the MTZ, indicating that the Indian lithosphere has subducted or detached into the MTZ or even the lower mantle (Huang et al., 2015, 2019; Lei and Zhao, 2016; Li et al., 2008; Liang et al., 2012; Peng et al., 2016; Replumaz et al., 2013). In addition, a locally thickened MTZ resulting from the depressed d660 was measured based on stacked receiver functions (Duan et al., 2015, 2017; Yue et al., 2012) and triplicate waveform modeling (Chen and Tseng, 2007), which confirmed that the cold Indian lithosphere subducted into the MTZ, leading to the decreased temperature and thickened MTZ.

Magmatic rocks were widely emplaced in the northern Qiangtang and Songpan-Gantze blocks from the Eocene to Miocene, far from the collision front (Fig. 1) (Guo and Wilson, 2019). As the lithospheric

* Corresponding authors.
E-mail addresses: gomijianxu@gmail.com (M. Xu), huangz@nju.edu.cn (Z. Huang), lswang@nju.edu.cn (L. Wang).

https://doi.org/10.1016/j.pepi.2020.106452
Received 26 November 2019; Received in revised form 22 February 2020; Accepted 22 February 2020
Available online 24 February 2020
0031-9201/

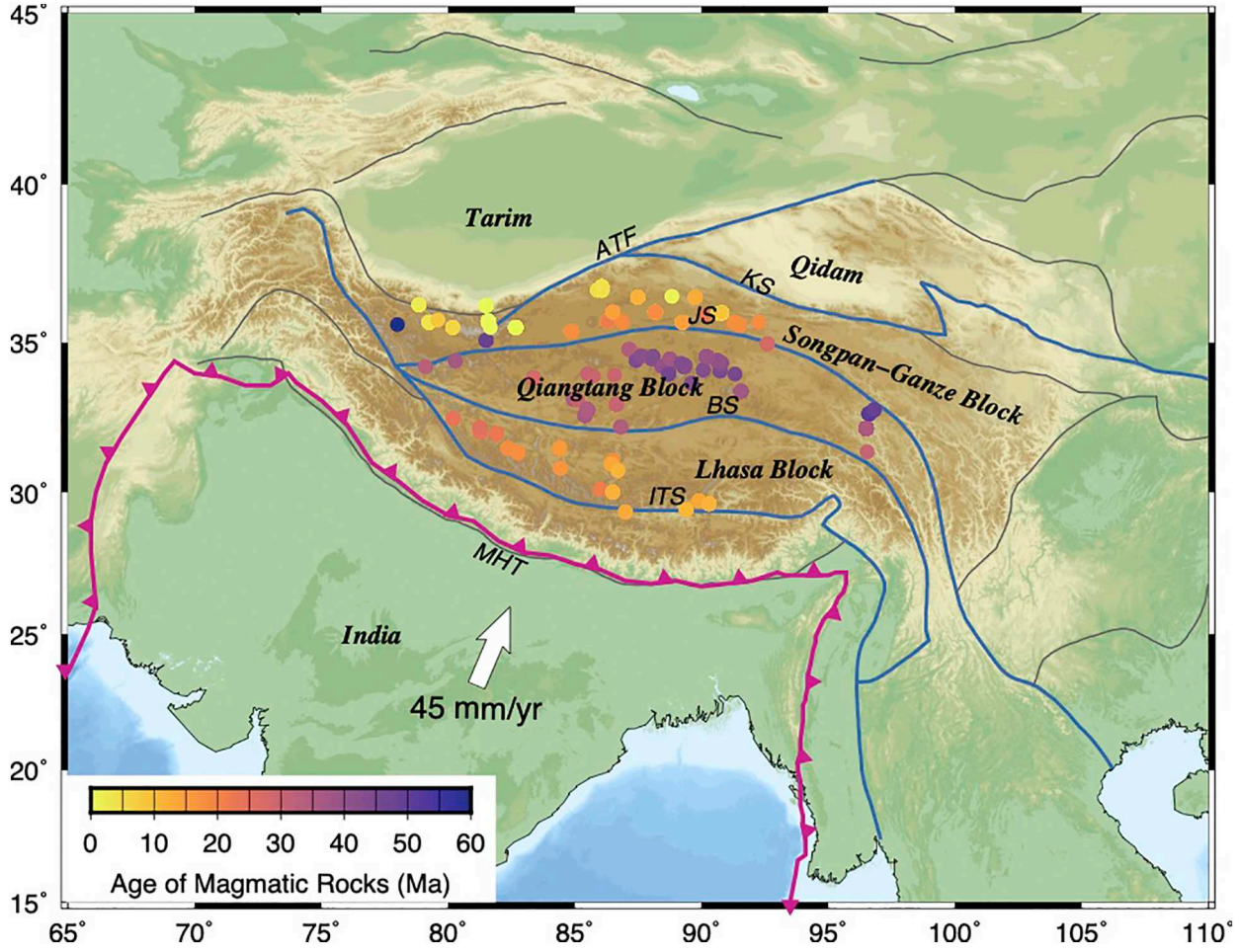

Fig. 1. Topography, tectonics and suture zones in the Tibetan Plateau and surrounding areas. Magenta lines with triangles represent plate boundary between the Indian and Eurasian plates; gray lines represent major faults; the suture zone in the Tibet are highlighted in blue. Colored circles denote ages of magmatic rocks distributions (Guo and Wilson, 2019). Acronyms: MHT, Main Himalaya Thrust; ITS, Indus-Tsangpo suture; BS, Bangong-Nujiang suture; JS, Jinshajiang suture; KS, Kunlun suture; ATF, Altyn Tagh fault. (For interpretation of the references to colour in this figure legend, the reader is referred to the web version of this article.)

deformation has propagated northward, the lithospheric mantle of the North China block has subducted southward since the Eocene (Tapponnier et al., 2001; Yin and Harrison, 2000). Therefore, these volcanic rocks are considered to have originated from dehydration of the subducted North China block. In other words, it is suggested that the volcanos came from the crust or lithospheric mantle. However, the magmatic rocks are composed of slab-derived carbonated melt and depleted mid-oceanic ridge basalt (MORB) (Guo and Wilson, 2019), which indicates that the late Cenozoic volcanic activity in the Qiangtang and Songpan-Ganze block originated from the deeper upper mantle (i.e., asthenosphere) rather than the lithosphere. The origin of the magmatic rocks was not well constrained by geochemical studies in general. Geophysical studies revealed southward oblique interfaces in the upper mantle extending down to ~200 km, indicating the southward-subducted North China lithospheric mantle (Kind et al., 2002; Kosarev et al., 1999; Zhao et al., 2010). However, seismic tomography revealed that there are obvious low velocity anomalies beneath the Qiangtang and Songpan-Gantze blocks, extending down to ~300–400 km depth (Huang and Zhao, 2006; Lei and Zhao, 2016; Liang et al., 2012; Wang et al., 2019; Wei et al., 2012; Wittlinger et al., 1996). Similar magmatic rocks are found beneath the Lhasa block in south Tibetan Plateau (Fig. 1). They generally have low Sr/Nb ratios, enrichments of SiO_2 and K_2O and depletion of Ca in olivine phenocrysts, indicating the composite of silicate sediment from the subducted Indian plate (Guo and Wilson, 2019).

Receiver functions (Langston, 1979), which are sensitive to lateral variations of the d410 and d660, are widely used to image MTZ structures under a seismic array (e.g., Eagar et al., 2010; Huang et al., 2014; Li and Yuan, 2003; Mulibo and Nyblade, 2013; Xu et al., 2018). Since 1991, many broadband seismic stations have been deployed in the central Tibetan Plateau. Thus, dense d410 and d660 pierce points would present an MTZ structure with higher resolution using the receiver function method. In this study, we collected all available seismic records from the Tibetan Plateau to image high-resolution d410 and d660 topography using P-wave receiver functions (PRFs).

2. Data and method

We collected seismic records from 15 temporary broadband seismic stations deployed by Nanjing University during 2013–2015 (brown triangles in Fig. 2) and another 459 stations from 11 seismic arrays: GSN (2002–2018), GANSSER (2013–2014), Bhutan PASSCAL (2002 – 2003), INDEPTH II (1994), INDEPTH III (1998–1999), INDEPTH IV (2007–2008), HIMNT (2001 – 2002), Hi-CLIMB (2004–2005), Namche Barwa Tibet (2003–2004), ASCENT (2007–2008), and the TP Broadband Experiment (1991–1992). We selected 2886 earthquakes with moment magnitudes (Mw) > 5.5 and epicenter distances between 30° and 90° (inset map in Fig. 2).

We adopted the process described by Xu et al. (2018) to calculate PRFs as follows: (1) the linear trend and mean shift of each selected seismic waveform were removed; (2) the waveforms were filtered with a third-order Butterworth filter from 0.05 to 2 Hz; (3) E-N components

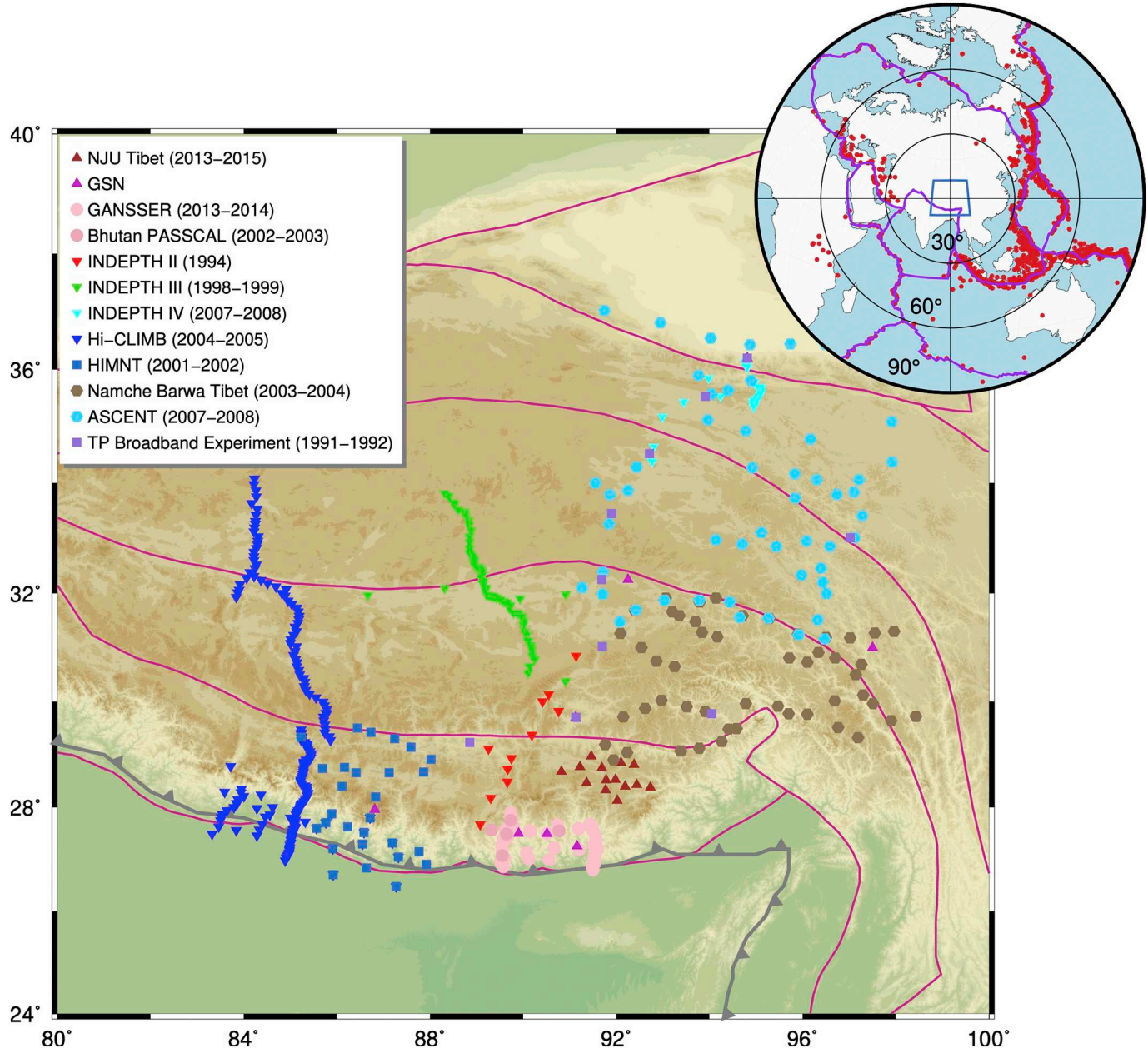

Fig. 2. Distributions of seismic stations in Tibet. Different symbols represent seismic stations from different arrays (See legend for details). Top-right inset shows teleseismic events used in this study. Red dots represent earthquakes; the blue box represents the study region; purple lines denote plate boundaries. (For interpretation of the references to colour in this figure legend, the reader is referred to the web version of this article.)

were rotated to T-R components; (4) the theoretical P arrival time was calculated for each event via the Taup toolkit (Crotwell et al., 1999); (5) records with signal-to-noise ratios < 7 dB were removed; (6) the data were trimmed from 10 s before the theoretical P arrival time to 120 s after the arrival; (7) the trimmed data of the *R* component were deconvoluted by those of the *Z* component using an iterative time-domain deconvolution method with a Gaussian factor of 0.5 (Ligorría and Ammon, 1999); (8) high quality PRFs were automatically and manually selected using the criteria of Xu et al. (2018). Ultimately, we obtained 40,336 PRFs. We stacked all the PRFs in 1° bins of epicentral distance and sorted them to check the quality of the PRFs (Fig. 3). The P410s and P660s were very clear and fit well with the theoretical Ps–P time difference, indicating that the signals were strong in the waveforms.

To reduce the noise and scattering effects, we converted time traces of all PRFs into depth traces and then stacked them using the CCP stacking technique (Dueker and Sheehan, 1997; Eagar et al., 2010; Huang et al., 2014; Xu et al., 2018). We calculated the Ps–P time difference and the locations of pierce points at an interval of 1 km (from depths of 300 to 800 km) with the AK135 reference model (Kennett et al., 1995). Fig. 4a and b shows the distributions of pierce points at 410 and 660 km in this study region, respectively. To suppress the influence of the velocity heterogeneities of the upper mantle on the d410 and d660 topographies, we used different three-dimensional (3D) velocity models (Kustowski et al., 2008; Liang et al., 2016; Simmons et al., 2010; Wang et al., 2019; Wei et al., 2012) to correct the Ps–P time difference (Xu et al., 2018). In time-to-depth conversions, the amplitudes at each depth were linearly interpolated by the Ps–P time difference from time traces of the PRFs.

We set up two-dimensional grid bins in the study region with a lateral interval of 0.5° and radius of 75 km (Fig. 4c and d). The amplitudes with pierce points falling in each bin were stacked with the bootstrap method (Efron and Tibshirani, 1986). The mean amplitude

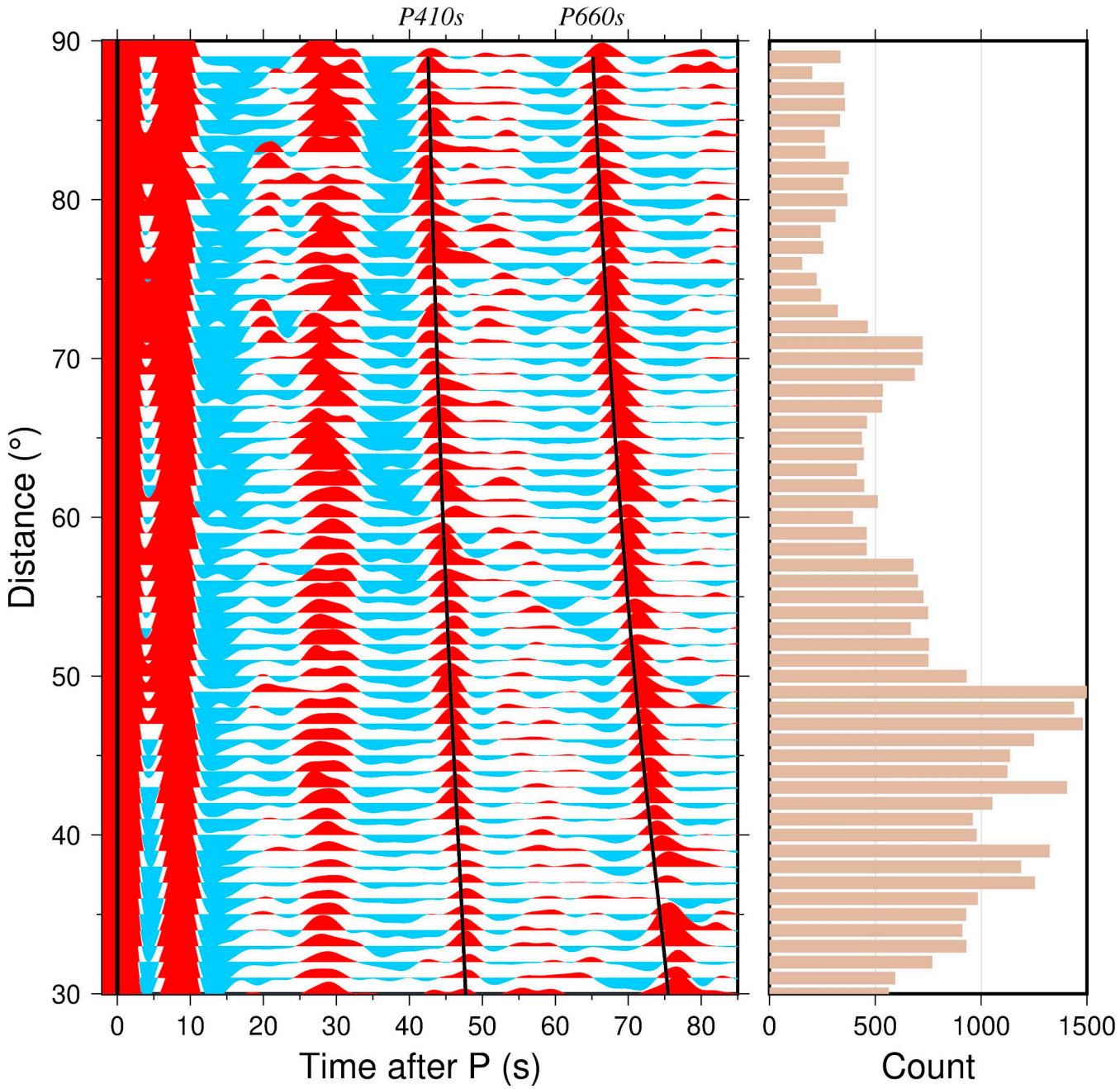

Fig. 3. (a) Stacked PRFs arranged by epicentral distance. Red and blue colors denote positive and negative peaks, respectively. Black lines show theoretical Ps-P time difference for P410s and P660s predicted by the AK135 model. (b) Number of PRFs in each epicentral distance. (For interpretation of the references to colour in this figure legend, the reader is referred to the web version of this article.)

and the 95% confidence interval of each bin were calculated from 2000 bootstrap results. We only kept bins with > 60 Ps piercing rays and with low boundary of confidence intervals > 0 after the bootstrap analysis (Fig. 4c and d).

3. Results

Fig. 5a and b (Model I) shows the d410 and d660 topographies after CCP stacking with the 1D AK135 model, respectively. The d410 varied between 382 km and 439 km, and the d660 varied between 633 km and 689 km. The d410 was predominantly relatively flat under the Lhasa block but deepened to over 430 km beneath the Qiangtang and Songpan-Ganze blocks; the d660 was flat under the Qiangtang block (between 91°E and 94°E) and apparently deepened to over 680 km under the Lhasa block (between 90°E and 94°E). Calculated as the difference between the d410 and d660 depths (Fig. 5c), the MTZ thickness showed strong lateral heterogeneities in central Tibet (between 92°E and 95°E). The MTZ thinned to ~230 km because of a ~20 km depression of the d410 under the Qiangtang and Songpan-Ganze blocks, located under the observed Late Cenozoic volcanic rocks (Guo and Wilson, 2019). In the middle of the Lhasa block, the MTZ thickened to > 270 km, located at the front of the northward subduction of the Indian lithosphere as revealed by seismic tomography (Chen et al., 2017; Lei and Zhao, 2016; Li et al., 2008; Liang et al., 2012; Replumaz et al., 2013; Wang et al., 2019).

In the Tibetan Plateau, the structures in the upper mantle are complex with strong lateral heterogeneities. There are a wide range of high velocity anomalies denoting subducted Indian lithosphere and low

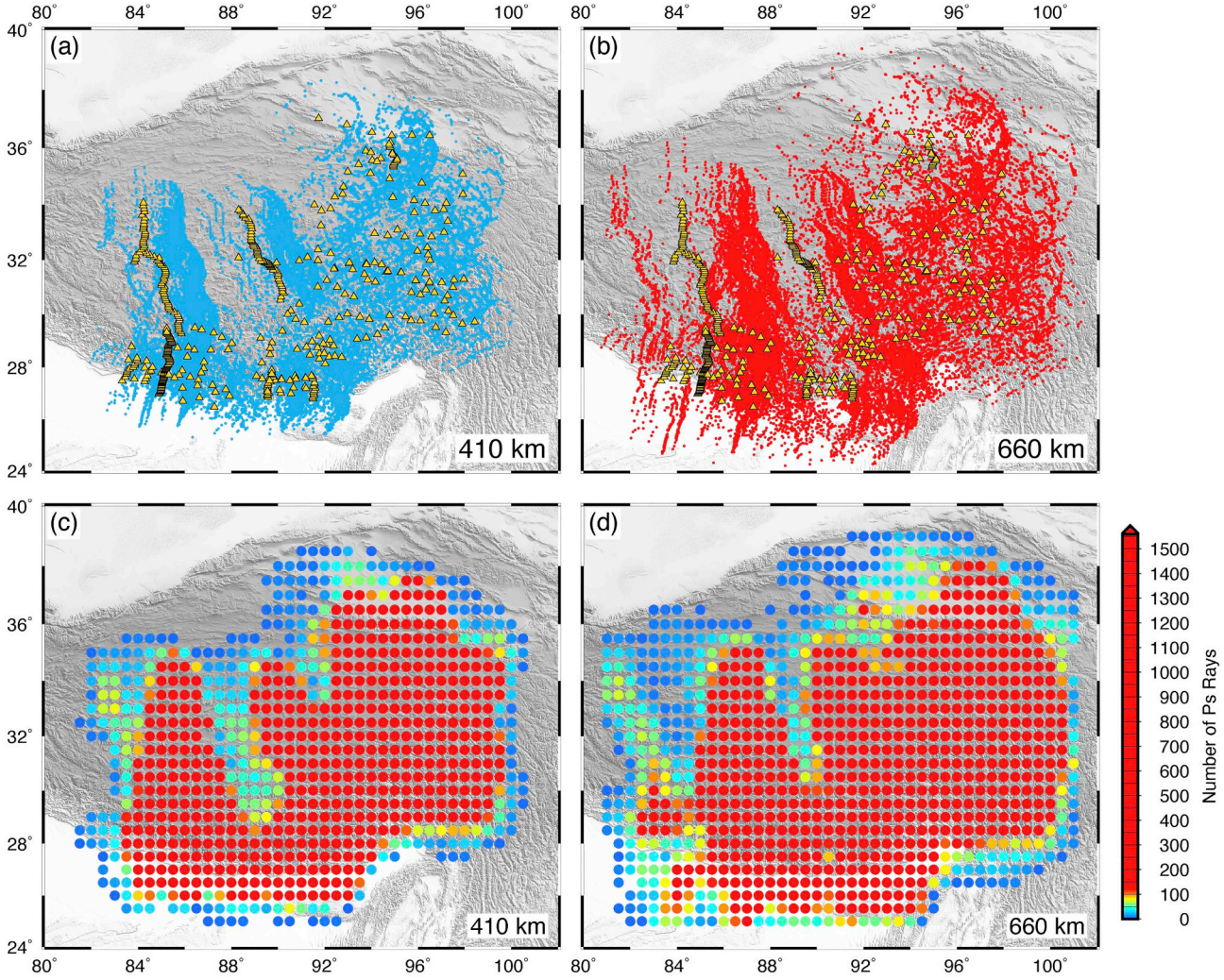

Fig. 4. (a and b) Blue and red dots denote Ps piercing points at 410 km and 660 km, respectively. (c and d) Number of piercing points within circular bins where the d410 and d660 peaks were selected. (For interpretation of the references to colour in this figure legend, the reader is referred to the web version of this article.)

velocity anomalies representing upwelling (Huang et al., 2015, 2019; Lei et al., 2019; Lei and Zhao, 2016; Li et al., 2008; Liang et al., 2012, 2016; Replumaz et al., 2013; Wang et al., 2019; Wei et al., 2012; Zhang et al., 2015). The velocity anomalies in the upper mantle cause an illusion of d410 and d660 depth in time-to-depth conversion. The high-velocity anomalies in the upper mantle lead to shallower depths of the calculated d410 and d660, and the low velocity anomalies lead to greater depths. In Model I (Fig. 5a and b), both the d410 and d660 are uplifted by 10–20 km under the Main Himalaya. This uplift may be caused by the high-velocity Indian slab under the Main Himalaya.

To confirm the reliability of the dominant features of the MTZ structures in Model I (i.e., lateral variations of the MTZ thickness), we used five 3D velocity models to correct the Ps–P time differences of the PRFs. Fig. 5d–f (Model II) shows the lateral variations of the d410 and d660 topographies, and the MTZ thickness was corrected by using a global velocity model (Simmons et al., 2010). The same contents of Fig. 6a–c (Model III) and Fig. 6d–f (Model IV) were corrected using the regional and local P-wave velocity models, respectively (Wang et al., 2019; Wei et al., 2012). Because of a lack of S-wave velocity data in these two 3D velocity models (Wang et al., 2019; Wei et al., 2012), we constructed an S-wave velocity model according to $dlnV_P/dlnV_S$ based on the relationship between mantle temperature and seismic velocity (Cammarano et al., 2003). Synthetic tests have shown that an S-wave velocity model constructed based on this $dlnV_P/dlnV_S$ relationship can restore the d410 and d660 depths while correcting the effects of upper-mantle velocity anomalies (Xu et al., 2018). We also collected the S-wave velocity model of Eurasia (Model V) (Kustowski et al., 2008) (the P-wave model was constructed by the above method) (Fig. 7a–c) and the P and S velocity models (< 400 km depth) of the Tibetan Plateau (Model VI) for Ps–P time difference correction (Liang et al., 2016) (Fig. 7d–f). The MTZ thickness in Models II–VI showed dominant features similar to those in Model I, although the d410 and d660 topographies were notably different.

Without Ps–P time correction using 3D models, the velocity anomalies in the upper mantle influence both the d410 and d660. Therefore, the d410 and d660 depths in the same bin showed strong positive correlation with a correlation coefficient of 0.69 (Fig. 8a). After the time corrections, the corresponding correlation coefficients were reduced to 0.56, 0.62, 0.56, 0.45 and 0.58 in Models II–VI, respectively (Fig. 8b–f). These reduced correlations suggest that some effects of the velocity anomalies in the upper mantle were removed by the time correction using the 3D velocity models. However, there are remaining correlation, which may result from the limited resolution of the velocity models and therefore the errors in time-to-depth conversions.

We constructed a new model of the MTZ thickness by stacking the results obtained with different velocity models (Fig. 9a). The stacked MTZ thickness further highlights the common features in different models while suppressing the differences. In the stacked model, the MTZ thickens to ~ 270 km under the Lhasa block (between 92°E and 96°E) and thins to ~230 km under the Qiangtang and Songpan-Ganze

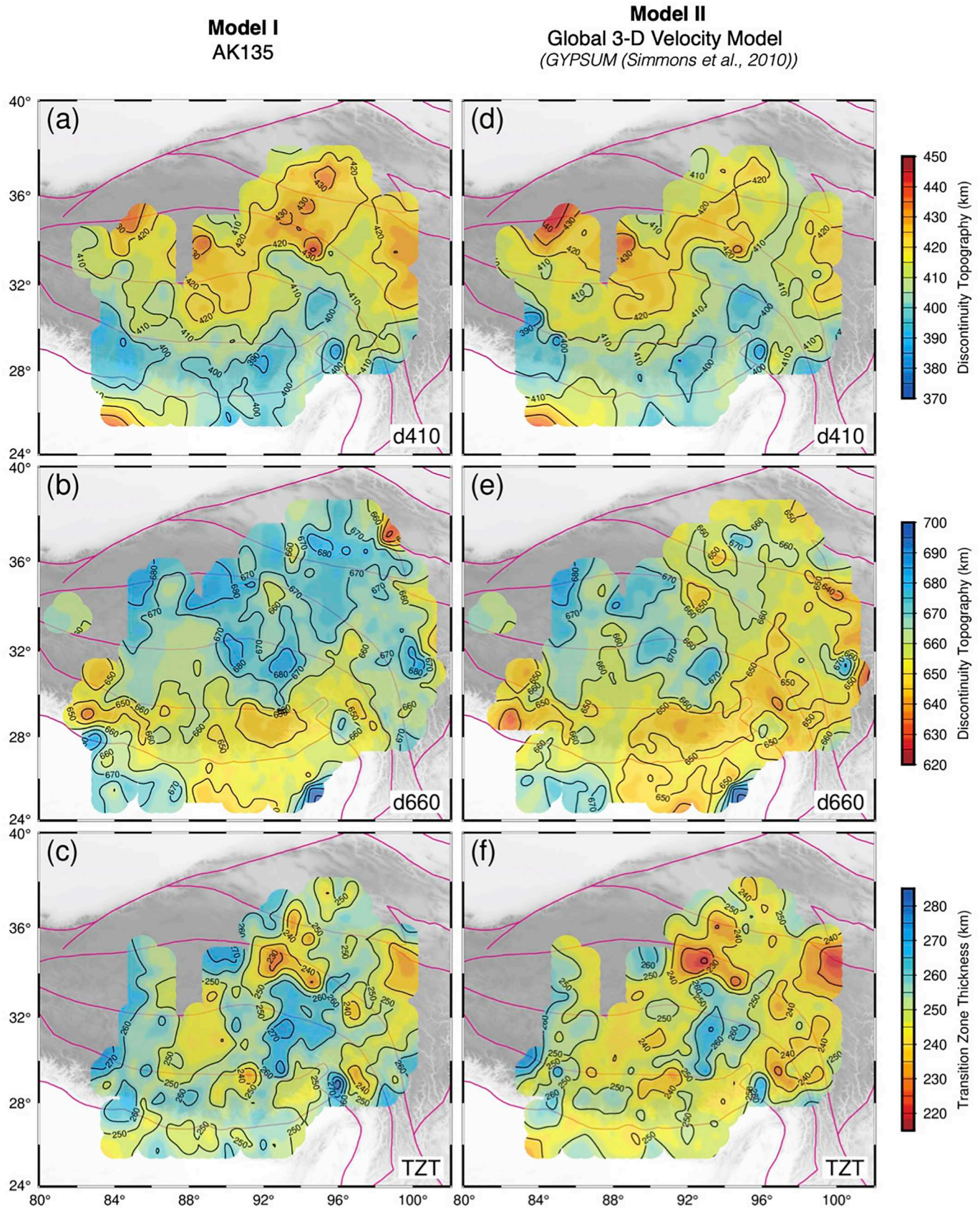

Fig. 5. (a–c) Topographies of the d410, d660 and MTZ thickness derived by the AK135 model. (d–f) The same as (a–c) but for the results derived by a global 3D velocity model (Simmons et al., 2010).

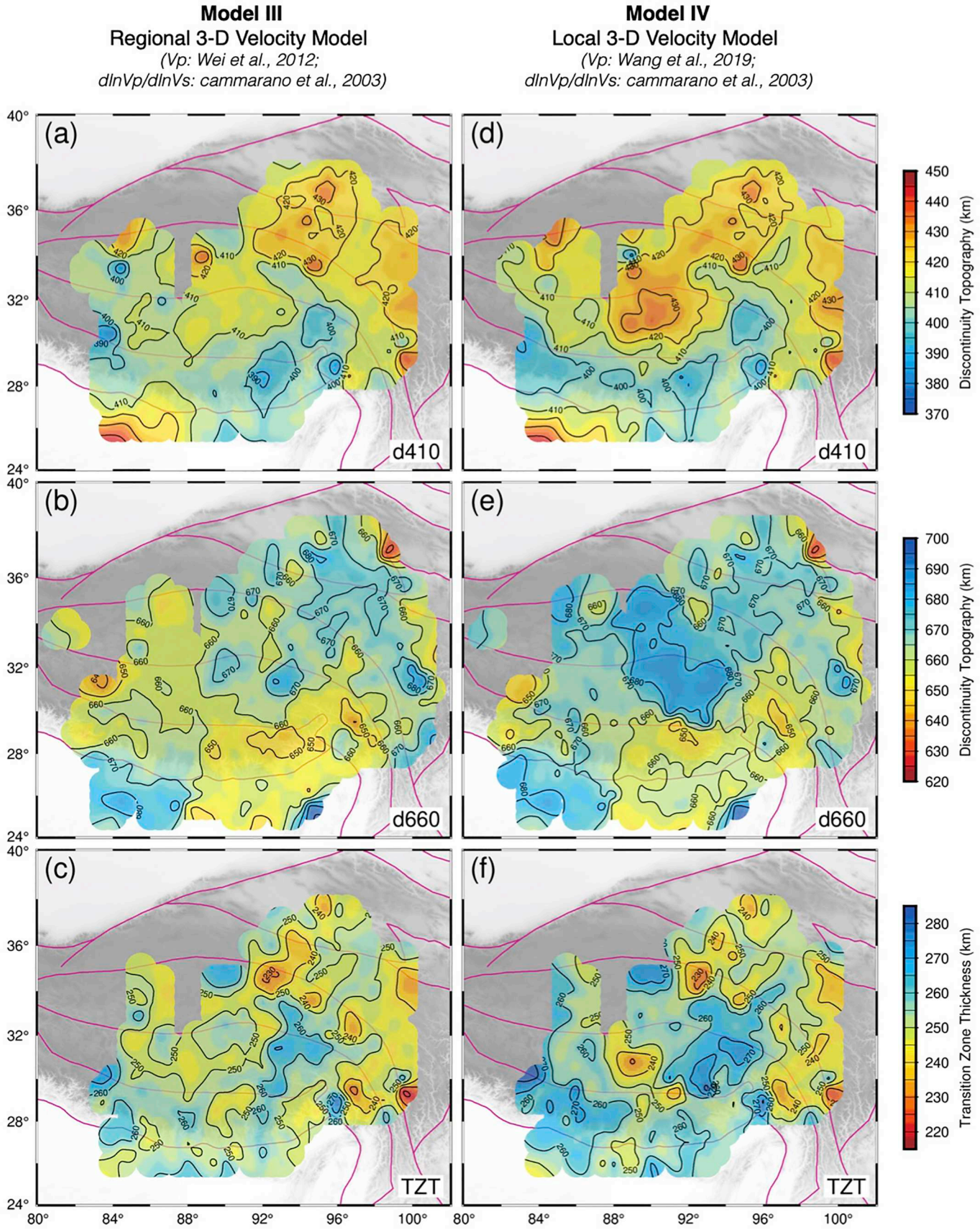

Fig. 6. The same as Fig. 5 but for the results derived by a regional (Wei et al., 2012) and local (Wang et al., 2019) 3D velocity models.

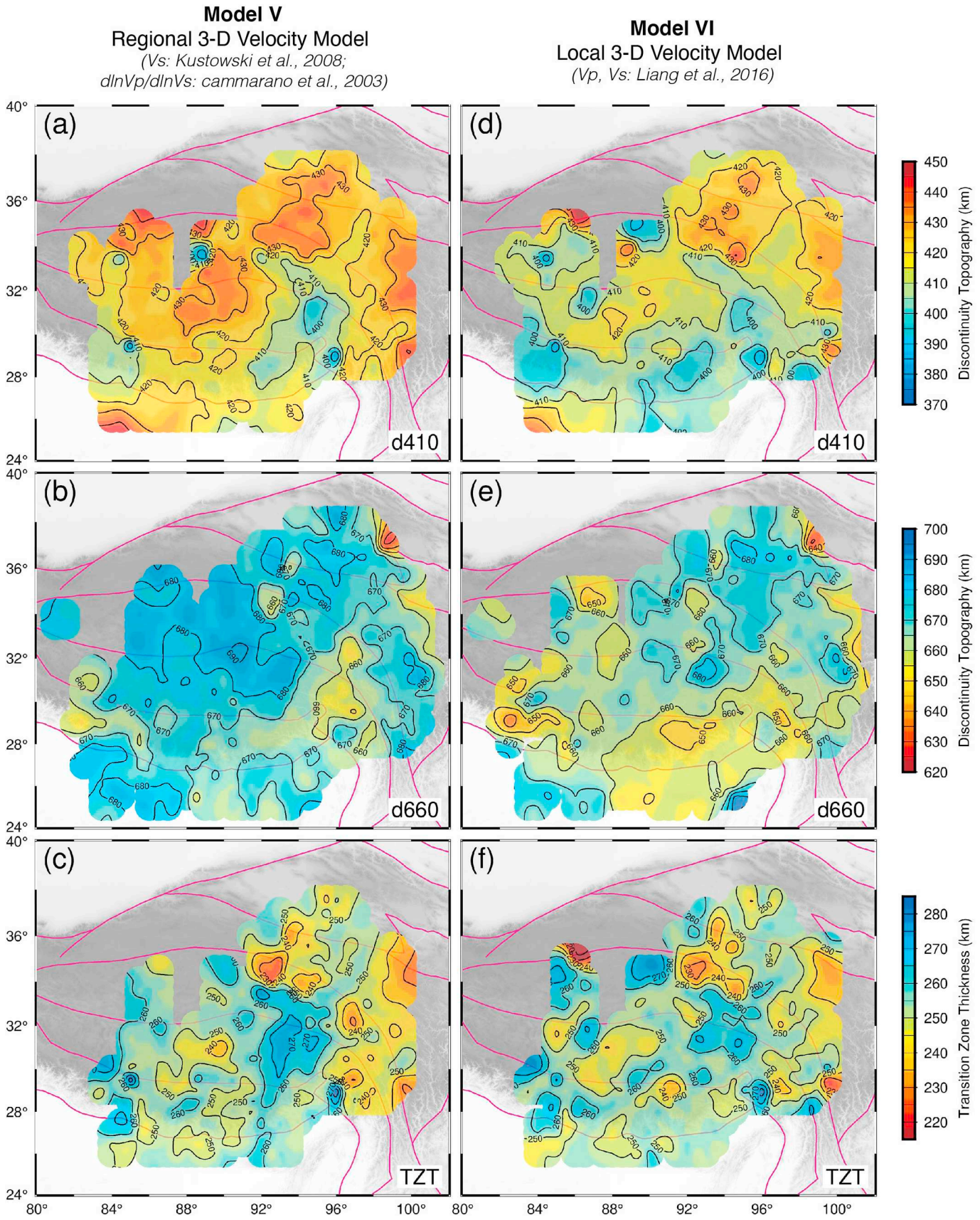

Fig. 7. The same as Fig. 5 but for the results derived by a regional (Kustowski et al., 2008) and local (Liang et al., 2016) 3D velocity models.

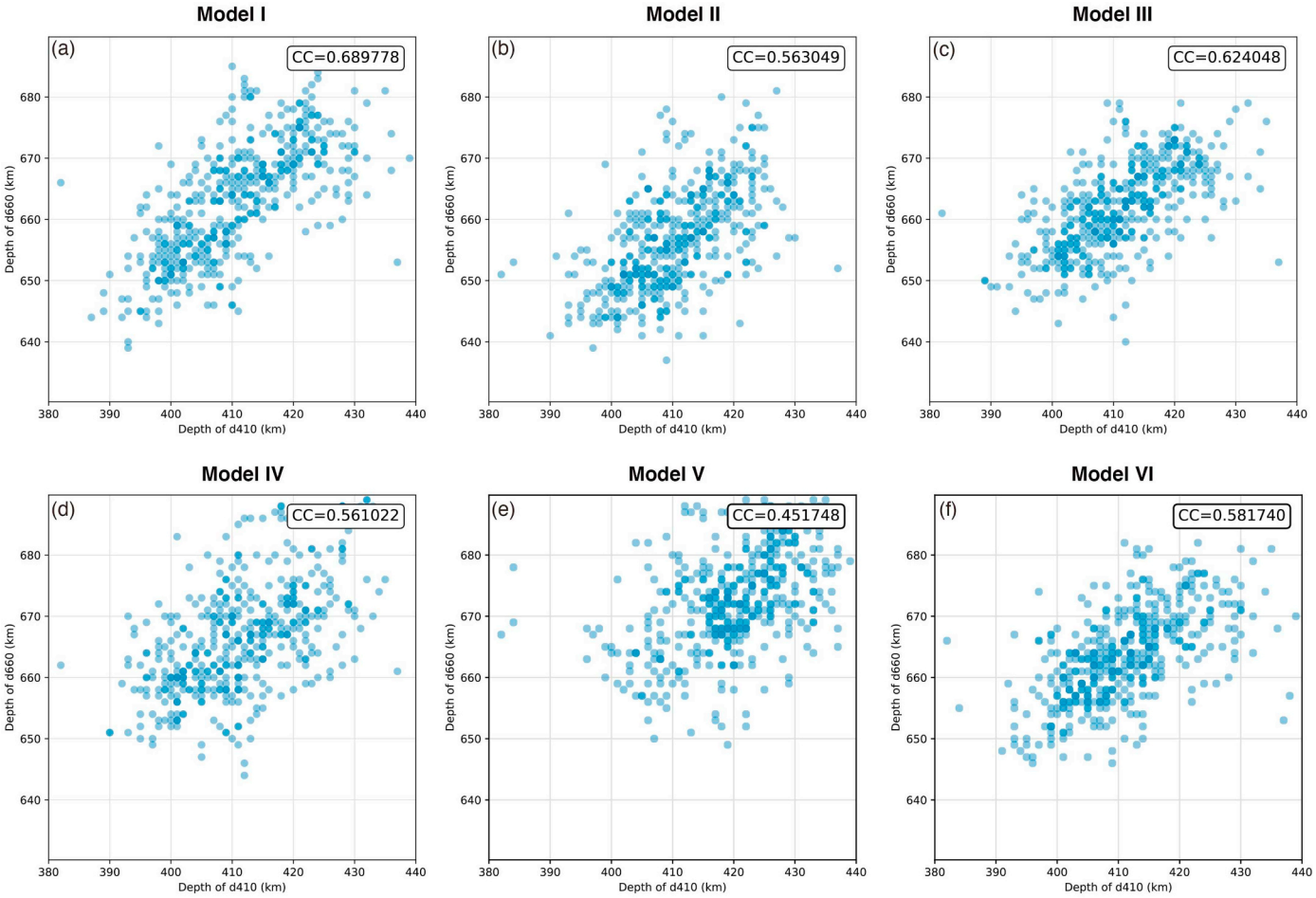

Fig. 8. The correlation between d410 and d660 depths in Model I–VI.

blocks (between 91°E and 95°E). In other regions, the MTZ thickness is close to the global average value of ~250 km.

4. Discussion

4.1. Comparison with tomographic results

The Indian lithosphere has been colliding with the Eurasian plate since the Eocene. Confirmed by geological and geophysical studies, the Indian lithosphere has subducted into the upper mantle under the Tibet Plateau (e.g., Huang and Zhao, 2006; Li et al., 2008; Liang et al., 2016; Pitard et al., 2018; Tapponnier et al., 2001; Wang et al., 2019; Webb et al., 2017; Yin and Harrison, 2000). The subducted slab has even detached into the upper mantle or the MTZ (e.g., Chen et al., 2017; Webb et al., 2017). However, the extending depth of the subducting slab is still debated. Regional tomographic images suggest that the Indian slab has been subducted down to ~200 km with a small dip angle (Huang and Zhao, 2006; Kustowski et al., 2008; Wei et al., 2012). In contrast, local tomographic images indicate that the slab has been subducted into the MTZ or has even stagnated there (Chen et al., 2017; Lei and Zhao, 2016; Liang et al., 2016; Nunn et al., 2014; Replumaz et al., 2013; Wang et al., 2019).

Our observations support the inference that the slab has reached the MTZ because the MTZ is thickened under the Lhasa block, which has high velocity anomalies beneath it. In contrast, the MTZ is thinned in regions with low-velocity anomalies in the upper mantle (Chen et al., 2017; Li et al., 2008; Liang et al., 2016; Wang et al., 2019). To further compare the MTZ structures with velocity anomalies, we stacked the PRFs (based on Model IV) along a profile across areas where the MTZ thickness changed significantly (Fig. 9b and c). The topographies of the d410 and d660 show strong correlations with P-wave velocity anomalies (background in Fig. 9c) (Wang et al., 2019). With high velocity anomalies, the MTZ under the Lhasa block is significantly thickened because of the depression of the d660. In contrast, with low-velocity anomalies extending down to 200 km, a depressed d410 and thinned MTZ are obvious under the Qiangtang block. The notably heterogeneous MTZ thickness and the upper-mantle velocity indicate that the subducted Indian slab has affected the mineral phase transition at the d660, and, at the same time, the hot upwelling under the Qiangtang and Songpan-Ganze blocks likely originates from the MTZ.

4.2. Subduction of the Indian plate

While the cold slab revealed by the high-velocity anomalies subducted into (or through) the MTZ, the MTZ thickness changed because the mineral phase transitions across both the d410 and d660 are influenced by the slab. Assuming that the Clapeyron slope of the olivine to wadsleyite transition is 3.6 to 4.0 MPa/K^{-1}, and that the Clapeyron slope of the ringwoodite to bridgmanite phase transition is −1.0 to −2.0 MPa/K^{-1} (Bina and Helffrich, 1994; Fei et al., 2004; Frost, 2008; Katsura et al., 2004), we speculate that a 20 km MTZ thickening under the Tibetan Plateau indicates a temperature anomaly of ~250–340 K. This value is basically consistent with previous observations in southeastern Tibet (Xu et al., 2018), where the subducted Indian slab affects the mineral phase transition across the d410 and/or d660.

The results of this study indicate significant MTZ thickening between longitudes of 92° and 96° (Fig. 10). Yue et al. (2012) used a local seismic array and also found MTZ thickening in similar areas. Duan

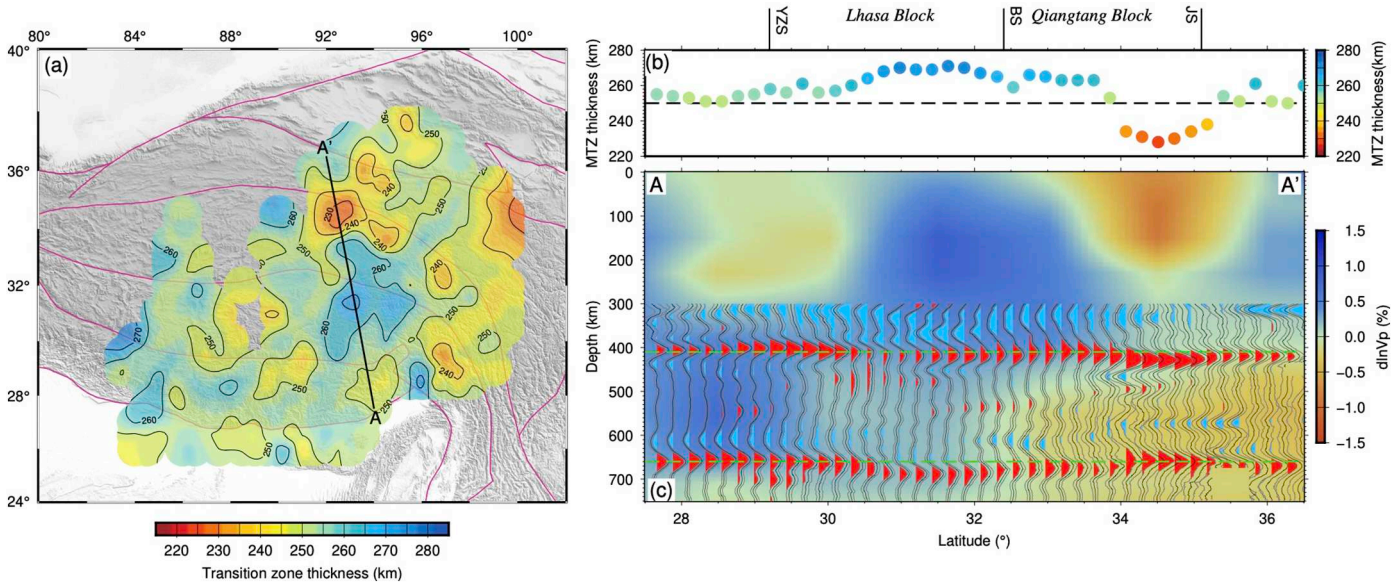

Fig. 9. (a) Average MTZ thickness with all models. (b) MTZ thickness at each bin along profile AA' shown in (a). (c) CCP stacked PRFs along profile AA'. Blue and red colors in background denote high and low P-wave velocity anomalies, respectively. Gray lines denote the 95% confidence intervals of stack PRFs. Black lines denote mean stacked PRFs. Red and blue colors denote positive and negative peaks. (For interpretation of the references to colour in this figure legend, the reader is referred to the web version of this article.)

et al. (2017) imaged the MTZ structures beneath central Tibet using an exclusive data set and found two thickened regions between 90° and 92° beneath the Lhasa and Qiangtang blocks, respectively (black dashed curves in Fig. 10). Triplicated waveform modeling implied that a notable anomaly of high P-wave velocity in the MTZ under the Qiangtang block between longitudes of 85° and 90°, which the d660 of the model was depressed by ~15 km (Chen and Tseng, 2007; Tseng and Chen, 2008). Combining these results with our new MTZ images, we suggest that the d660 is depressed and the MTZ thickened under the Tibetan Plateau, especially under the Lhasa block.

The distribution of the subducted slab in the upper mantle indicated by seismic tomography is still issuable. Regional and local tomographic results suggest subduction in the upper mantle under the middle and western Lhasa block (e.g., Li et al., 2008; Wang et al., 2019; Zhang et al., 2012, 2015), where the MTZ thickening was also observed in receiver function and triplicated waveform modeling (Chen and Tseng, 2007; Duan et al., 2017; Tseng and Chen, 2008). However, local tomographic studies indicated that the Indian plate subducted to the d410 or into the MTZ in the eastern Lhasa block (Lei and Zhao, 2016; Lei et al., 2019; Nunn et al., 2014; Peng et al., 2016). MTZ thickening was observed in a similar region (92°E–96°E), consistent with the deep subduction shown in the tomographic images. These results confirm that the Indian slab has at least subducted down into the MTZ.

4.3. Volcanic activity in the Tibetan plateau

Late Cenozoic magmatic rocks are widely distributed in the Qiangtang and Songpan-Gantze blocks (Fig. 1). Seismic tomography revealed that the low velocity anomalies beneath these blocks extend from the MTZ to the surface (Chen et al., 2017; Liang et al., 2016; Wang et al., 2019), which indicates that the volcano-related heat upwelling originated from the deeper upper mantle rather than from the lithosphere. Because of a significant d410 depression, the MTZ is thinned by ~20 km under the Qiangtang and Songpan-Gantze blocks (between 92°E and 95°E) where low velocity anomalies are obvious in the P-wave tomography (Fig. 9) (Wang et al., 2019). Therefore, we suggest that the upwelling originated from the MTZ and influenced at least the mineral phase transition across the d410 by increasing the temperature.

Magmatic rocks are widespread in the plateau (colored dots in Fig. 10), but different groups of the magmatic rocks have been distinguished by isotopic geochemical studies (Guo and Wilson, 2019). The magmatic rocks in the Lhasa block are composed of the silicate sediment. It may be directly related to the northward subduction of the Indian plate in the upper mantle above 410 km. The flat or slightly uplifted D410 we imaged under the Lhasa block suggest no notable anomaly of high temperature in the MTZ. The result confirms that the magmatic rocks in the Lhasa block originate from the upper mantle, i.e., lithosphere or asthenosphere. In contrast, the magmatic rocks in the Qiangtang and Songpan-Ganze block are distributed in front of the subducted slab rather than above the slab. This phenomenon means that this volcanic activity was not directly formed by the dehydration of the subducted Indian slab. Isotopic geochemical studies indicated that these magmatic rocks are composed of the Indian carbonated melt and the depleted MORB of the Tibetan Plateau (Guo and Wilson, 2019). The depleted MORB components in the mantle source of the xenoliths indicate native material of the deep upper mantle following mantle upwelling to the surface. The thinner MTZ due to depressed d410 indicates that the upwelling originated from the MTZ. However, the flat d660 suggests that the mantle upwelling does not extend deeper in the lower MTZ and low mantle. Li et al. (2016) used a thermodynamic model to numerically simulate the continental collision of the Tibetan Plateau. The results demonstrated that the Indian lithospheric subduction into the upper mantle triggers upwelling through the upper mantle; this upwelling can weaken the lithosphere and reach the surface. Therefore, we infer that the subducted Indian plate (into the MTZ) induced the upwelling from the MTZ, resulting in the thinning of the MTZ and low velocity anomalies in the upper mantle.

We have proposed an improved model of upper-mantle dynamics for the Indian–Asian collision (Fig. 11). The Indian lithosphere subducts northward accompanying the Indian–Asian collision. Subducting into the MTZ or even sinking into the lower mantle, the subducted Indian lithosphere changes the temperature in the MTZ, resulting in thickening of the MTZ under Tibet. The subduction triggers mantle upwelling from the MTZ. The increasing temperature induces a depression of the d410 and thinning of the MTZ. This model not only shows that the Indian plate has subducted into the MTZ, but also confirms that the magmatic rocks exposed in the Qiangtang and Songpan-Gantze blocks originated from the MTZ.

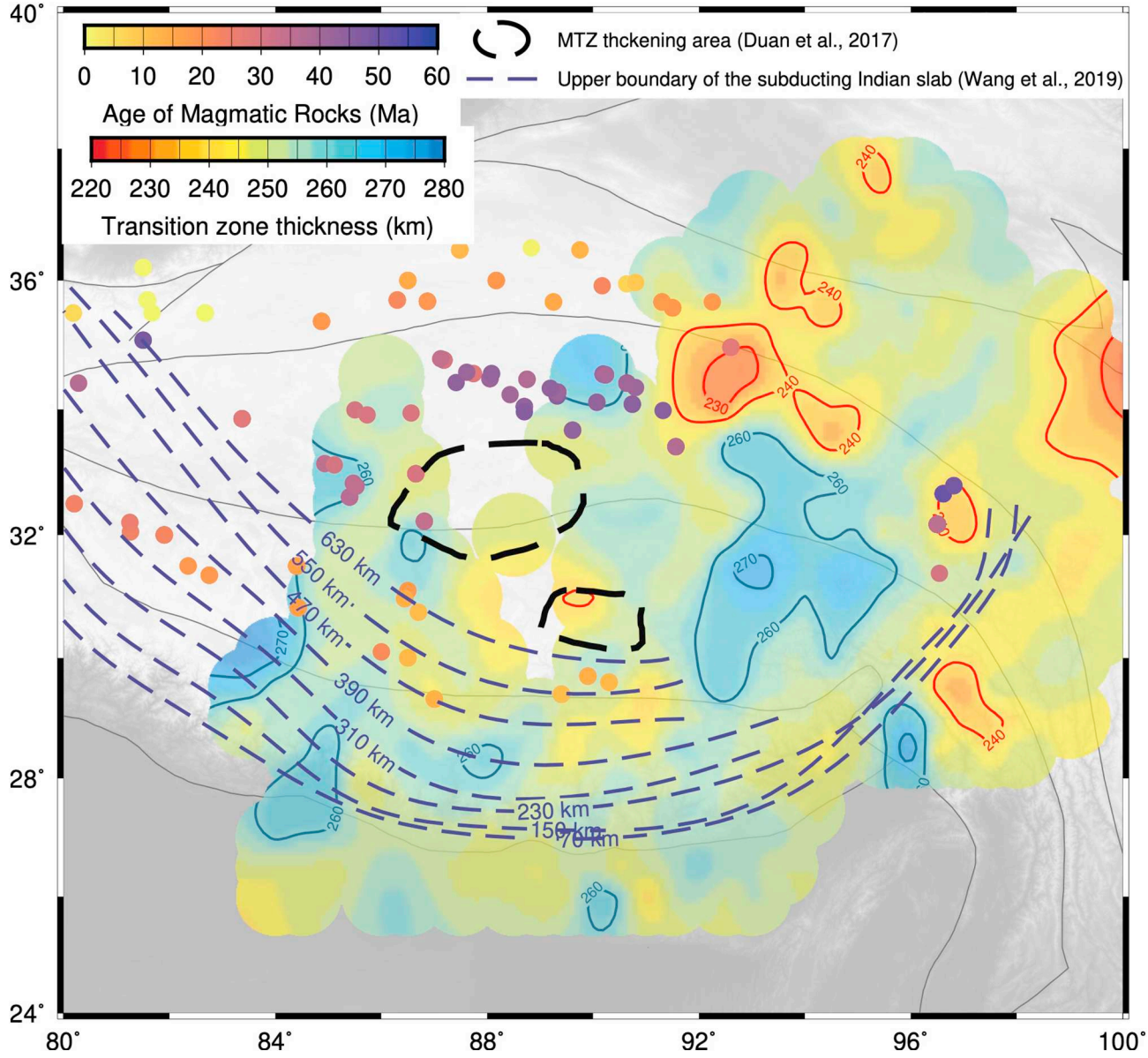

Fig. 10. Comparison of the MTZ thickness with other geophysical observations. The black dashed curves denote areas where the thickened MTZ was found by Duan et al. (2017). The blue dashed lines denote upper boundary of the subducting Indian slab (Wang et al., 2019). The colored dots represent magmatic rocks (Guo and Wilson, 2019). (For interpretation of the references to colour in this figure legend, the reader is referred to the web version of this article.)

5. Conclusion

To study the MTZ structures beneath the central Tibetan Plateau, we collected as many seismic records as possible for imaging the topographies of the d410 and d660 by the receiver function and CCP stacking methods. We corrected Ps–P time differences with 3D velocity models to reduce the effects of upper-mantle velocity heterogeneities. The results exhibit a thickened MTZ under the Lhasa block and a thinned MTZ under the Qiangtang and Songpan-Ganze blocks, consistent with the high velocity anomalies in the MTZ and low velocity anomalies in the upper mantle, respectively. Based on these results combined with the results of isotopic geochemistry and numerical simulation, we suggest that the Indian plate subducted northward into the MTZ and induced upwelling from the MTZ to the surface.

CRediT authorship contribution statement

Mijian Xu:Methodology, Software, Formal analysis, Writing - original draft.**Zhouchuan Huang**:Conceptualization, Writing - review & editing.**Liangshu Wang**:Supervision, Project administration.**Mingjie Xu**:Writing - review & editing.**Ning Mi**:Resources, Data curation.**Dayong Yu**:Resources.

Declaration of competing interest

The authors declare that they have no known competing financial interests or personal relationships that could have appeared to influence the work reported in this paper.

Acknowledgments

The seismic data were provided by the IRIS Data Management Center. This study was supported by the National Natural Science Foundation of China (41674049, 41674044), and by the National Key Research and Development Program of China (2016YFC0600302). Most figures were generated using GMT 6 (Wessel et al., 2019). We are

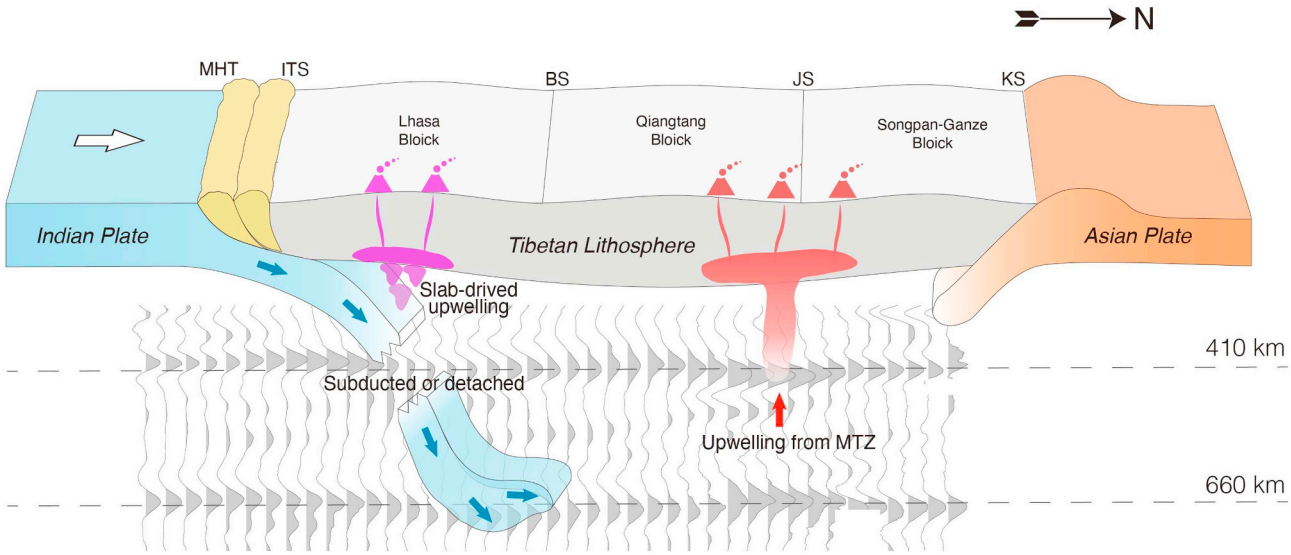

Fig. 11. Model of upper-mantle dynamics together with the MTZ structures in Tibet. Waveforms with gray peaks represent stacked PRFs along profile AA' (Fig. 8c). Blue and red arrows denote the Indian plate subduction and the mantle upwelling, respectively. (For interpretation of the references to colour in this figure legend, the reader is referred to the web version of this article.)

grateful to Dr. Zewei Wang, Prof. Xiaofeng Liang, and Prof. Wei Wei for providing their tomographic results. We thank Prof. Vernon Cormier (the editor) and three anonymous reviewers for their constructive comments.

References

Bina, C.R., Helffrich, G., 1994. Phase transition Clapeyron slopes and transition zone seismic discontinuity topography. Journal of Geophysical Research: Solid Earth 99, 15853–15860. https://doi.org/10.1029/94JB00462.

Brookfield, M.E., 1993. The Himalayan passive margin from Precambrian to Cretaceous times. Sediment. Geol. 84, 1–35. https://doi.org/10.1016/0037-0738(93)90042-4.

Burchfiel, B.C., Zhiliang, C., Hodges, K.V., Yuping, L., Royden, L.H., Changrong, D., Xujiene, 1992. The South Tibetan Detachment System. Extension Contemporaneous with and Parallel to Shortening in a Collisional Mountain Belt. Geological Society of America, Himalayan Orogen.

Burtman, V.S., Molnar, P.H., 1993. Geological and Geophysical Evidence for Deep Subduction of Continental Crust Beneath the Pamir. (Geological Society of America).

Cammarano, F., Goes, S., Vacher, P., Giardini, D., 2003. Inferring upper-mantle temperatures from seismic velocities. Phys. Earth Planet. Inter. 138, 197–222. https://doi.org/10.1016/S0031-9201(03)00156-0.

Chen, W.-P., Tseng, T.-L., 2007. Small 660-km seismic discontinuity beneath Tibet implies resting ground for detached lithosphere. J. Geophys. Res. 112, B05309. https://doi.org/10.1029/2006JB004607.

Chen, M., Niu, F., Tromp, J., Lenardic, A., Lee, C.-T.A., Cao, W., Ribeiro, J., 2017. Lithospheric foundering and underthrusting imaged beneath Tibet. Nat. Commun. 8, 15659. https://doi.org/10.1038/ncomms15659.

Crotwell, H.P., Owens, T.J., Ritsema, J., 1999. The TauP toolkit: flexible seismic travel-time and ray-path utilities. Seismol. Res. Lett. 70, 154–160. https://doi.org/10.1785/gssrl.70.2.154.

Duan, Y., Tian, X., Liu, Z., Zhu, G., Nie, S., 2015. Lithospheric detachment of India and Tibet inferred from thickening of the mantle transition zone. J. Geodyn. 97, 1–6. https://doi.org/10.1016/j.jog.2016.02.001.

Duan, Y., Tian, X., Liang, X., Li, W., Wu, C., Zhou, B., Iqbal, J., 2017. Subduction of the Indian slab into the mantle transition zone revealed by receiver functions. Tectonophysics 702, 61–69. https://doi.org/10.1016/j.tecto.2017.02.025.

Dueker, K.G., Sheehan, A.F., 1997. Mantle discontinuity structure from midpoint stacks of converted P to S waves across the Yellowstone hotspot track. Journal of Geophysical Research: Solid Earth 102, 8313–8327. https://doi.org/10.1029/96JB03857.

Eagar, K.C., Fouch, M.J., James, D.E., 2010. Receiver function imaging of upper mantle complexity beneath the Pacific Northwest, United States. Earth Planet. Sci. Lett. 297, 141–153. https://doi.org/10.1016/j.epsl.2010.06.015.

Efron, B., Tibshirani, R., 1986. Bootstrap methods for standard errors, confidence intervals, and other measures of statistical accuracy. Stat. Sci. 54–75.

England, P., Houseman, G., 1986. Finite strain calculations of continental deformation: 2. Comparison with the India-Asia collision zone. Journal of Geophysical Research: Solid Earth 91, 3664–3676.

Fei, Y., Orman, J.V., Li, J., van Westrenen, W., Sanloup, C., Minarik, W., Hirose, K., Komabayashi, T., Walter, M., Funakoshi, K., 2004. Experimentally determined postspinel transformation boundary in Mg2SiO4 using MgO as an internal pressure standard and its geophysical implications. Journal of Geophysical Research: Solid Earth 109. doi:https://doi.org/10.1029/2003JB002562.

Frederick, D.J., Millner, S.R., Chang, C., Sun, Y., Chang, C., Millner, Shackleton Robert, Frederick, Dewey John, Yin, Jixiang, 1988. The tectonic evolution of the Tibetan Plateau. Philosophical Transactions of the Royal Society of London. Series A, Mathematical and Physical Sciences 327, 379–413. https://doi.org/10.1098/rsta.1988.0135.

Frost, D.J., 2008. The upper mantle and transition zone. Elements 4, 171–176.

Gaetani, M., Jadoul, F., Erba, E., Garzanti, E., 1993. Jurassic and cretaceous orogenic events in the North Karakoram: age constraints from sedimentary rocks. Geol. Soc. Lond., Spec. Publ. 74, 39–52. https://doi.org/10.1144/GSL.SP.1993.074.01.04.

Guo, Z., Wilson, M., 2019. Late Oligocene–early Miocene transformation of postcollisional magmatism in Tibet. Geology. https://doi.org/10.1130/G46147.1.

Huang, J., Zhao, D., 2006. High-resolution mantle tomography of China and surrounding regions. J. Geophys. Res. 111. https://doi.org/10.1029/2005jb004066.

Huang, H., Wang, P., Mi, N., Huang, Z., Xu, M., Wang, L., Li, H., Yu, D., 2014. Lateral variations of the mantle transition zone structure beneath eastern China. Bull. Seismol. Soc. Am. 104, 1533–1539. https://doi.org/10.1785/0120130315.

Huang, Z., Zhao, D., Wang, L., 2015. P wave tomography and anisotropy beneath Southeast Asia: insight into mantle dynamics. J. Geophys. Res. Solid Earth 1–21. https://doi.org/10.1002/2015JB012098.Received.

Huang, Z., Wang, L., Xu, M., Zhao, D., Mi, N., Yu, D., 2019. P and S wave tomography beneath the SE Tibetan plateau: evidence for lithospheric delamination. Journal of Geophysical Research: Solid Earth 124, 10292–10308. https://doi.org/10.1029/2019JB017430.

Katsura, T., Yamada, H., Nishikawa, O., Song, M., Kubo, A., Shinmei, T., Yokoshi, S., Aizawa, Y., Yoshino, T., Walter, M.J., Ito, E., Funakoshi, K., 2004. Olivine-wadsleyite transition in the system (Mg,Fe)2SiO4. Journal of Geophysical Research: Solid Earth 109, B02209. doi:https://doi.org/10.1029/2003JB002438.

Kennett, B.L.N., Engdahl, E.R., Buland, R., 1995. Constraints on seismic velocities in the earth from traveltimes. Geophys. J. Int. 122, 108–124. https://doi.org/10.1111/j.1365-246X.1995.tb03540.x.

Kind, R., Yuan, X., Saul, J., Nelson, D., Sobolev, S.V., Mechie, J., Zhao, W., Kosarev, G., Ni, J., Achauer, U., Jiang, M., 2002. Seismic images of crust and upper mantle beneath Tibet: evidence for Eurasian plate subduction. Science 298, 1219–1221. https://doi.org/10.1126/science.1078115.

Kosarev, C., Kind, R., Sobolev, S.V., Yuan, X., Hanka, W., Oreshin, S., 1999. Seismic evidence for a detached indian lithospheric mantle beneath Tibet. Science 283, 1306–1309. https://doi.org/10.1126/science.283.5406.1306.

Kustowski, B., Ekström, G., Dziewoński, A.M., 2008. The shear-wave velocity structure in the upper mantle beneath Eurasia. Geophys. J. Int. 174, 978–992. https://doi.org/10.1111/j.1365-246X.2008.03865.x.

Langston, C.A., 1979. Structure under Mount Rainier, Washington, inferred from teleseismic body waves. Journal of Geophysical Research: Solid Earth 84, 4749–4762. https://doi.org/10.1029/JB084iB09p04749.

Lei, J., Zhao, D., 2016. Teleseismic P-wave tomography and mantle dynamics beneath Eastern Tibet. Geochem. Geophys. Geosyst. 17, 1861–1884. https://doi.org/10.1002/2016GC006262.

Lei, J., Zhao, D., Xu, X., Xu, Y.-G., Du, M., 2019. Is there a big mantle wedge under eastern Tibet? Phys. Earth Planet. Inter. 292, 100–113. https://doi.org/10.1016/j.pepi.2019.04.005.

Li, X., Yuan, X., 2003. Receiver functions in northeast China – implications for slab penetration into the lower mantle in northwest Pacific subduction zone. Earth Planet. Sci. Lett. 216, 679–691. https://doi.org/10.1016/s0012-821x(03)00555-7.

Li, C., van der Hilst, R.D., Meltzer, A.S., Engdahl, E.R., 2008. Subduction of the Indian lithosphere beneath the Tibetan Plateau and Burma. Earth Planet. Sci. Lett. 274,

157–168. https://doi.org/10.1016/j.epsl.2008.07.016.
Li, Z.-H., Liu, M., Gerya, T., 2016. Lithosphere delamination in continental collisional orogens: a systematic numerical study: dynamics of lithosphere delamination. J. Geophys. Res. Solid Earth 121, 5186–5211. https://doi.org/10.1002/2016JB013106.
Liang, X., Sandvol, E., Chen, Y.J., Hearn, T., Ni, J., Klemperer, S., Shen, Y., Tilmann, F., 2012. A complex Tibetan upper mantle: a fragmented Indian slab and no south-verging subduction of Eurasian lithosphere. Earth Planet. Sci. Lett. 333–334, 101–111. https://doi.org/10.1016/j.epsl.2012.03.036.
Liang, X., Chen, Y., Tian, X., Chen, Y.J., Ni, J., Gallegos, A., Klemperer, S.L., Wang, M., Xu, T., Sun, C., Si, S., Lan, H., Teng, J., 2016. 3D imaging of subducting and fragmenting Indian continental lithosphere beneath southern and central Tibet using body-wave finite-frequency tomography. Earth Planet. Sci. Lett. 443, 162–175. https://doi.org/10.1016/j.epsl.2016.03.029.
Ligorría, J.P., Ammon, C.J., 1999. Iterative deconvolution and receiver-function estimation. Bull. Seismol. Soc. Am. 89, 1395–1400.
Molnar, P., Tapponnier, P., 1975. Cenozoic tectonics of Asia : effects of a continental collision. Science 189, 419–426. https://doi.org/10.1126/science.189.4201.419.
Mulibo, G.D., Nyblade, A., 2013. Mantle transition zone thinning beneath eastern Africa: evidence for a whole-mantle superplume structure. Geophys. Res. Lett. 40, 3562–3566. https://doi.org/10.1002/grl.50694.
Nunn, C., Roecker, S.W., Tilmann, F.J., Priestley, K.F., Heyburn, R., Sandvol, E.A., Ni, J.F., Chen, Y.J., Zhao, W., 2014. Imaging the lithosphere beneath NE Tibet: Teleseismic P and S body wave tomography incorporating surface wave starting models. Geophys. J. Int. 196, 1724–1741. https://doi.org/10.1093/gji/ggt476.
Peng, M., Jiang, M., Li, Z.-H., Xu, Z., Zhu, L., Chan, W., Chen, Y., Wang, Y., Yu, C., Lei, J., Zhang, L., Li, Q., Xu, L., 2016. Complex Indian subduction style with slab fragmentation beneath the Eastern Himalayan Syntaxis revealed by teleseismic P-wave tomography. Tectonophysics 667, 77–86. https://doi.org/10.1016/j.tecto.2015.11.012.
Pitard, P., Replumaz, A., Funiciello, F., Husson, L., Faccenna, C., 2018. Mantle kinematics driving collisional subduction: insights from analogue modeling. Earth Planet. Sci. Lett. 502, 96–103. https://doi.org/10.1016/j.epsl.2018.08.050.
Replumaz, A., Guillot, S., Villaseñor, A., Negredo, A.M., 2013. Amount of Asian lithospheric mantle subducted during the India/Asia collision. Gondwana Res. 24, 936–945. https://doi.org/10.1016/j.gr.2012.07.019.
Replumaz, A., Funiciello, F., Reitano, R., Faccenna, C., Balon, M., 2016. Asian collisional subduction: a key process driving formation of the Tibetan Plateau. Geology 44, 943–946. https://doi.org/10.1130/G38276.1.
Royden, L.H., Burchfiel, B.C., van der Hilst, R.D., 2008. The geological evolution of the Tibetan Plateau. Science 321, 1054–1058. https://doi.org/10.1126/science.1155371.
Simmons, N.A., Forte, A.M., Boschi, L., Grand, S.P., 2010. GyPSuM: a joint tomographic model of mantle density and seismic wave speeds. Journal of Geophysical Research: Solid Earth 115. https://doi.org/10.1029/2010JB007631.
Tapponnier, P., Zhiqin, X., Roger, F., Meyer, B., Arnaud, N., Wittlinger, G., Jingsui, Y., 2001. Oblique stepwise rise and growth of the Tibet plateau. Science 294, 1671–1677. https://doi.org/10.1126/science.105978.
Tseng, T.-L., Chen, W.-P., 2008. Discordant contrasts of P- and S-wave speeds across the 660-km discontinuity beneath Tibet: a case for hydrous remnant of sub-continental lithosphere. Earth Planet. Sci. Lett. 268, 450–462. https://doi.org/10.1016/j.epsl.2008.01.038.
Wang, Z., Zhao, D., Gao, R., Hua, Y., 2019. Complex subduction beneath the Tibetan plateau: a slab warping model. Phys. Earth Planet. Inter. 292, 42–54. https://doi.org/10.1016/j.pepi.2019.04.007.
Webb, A.A.G., Guo, H., Clift, P.D., Husson, L., Müller, T., Costantino, D., Yin, A., Xu, Z., Cao, H., Wang, Q., 2017. The Himalaya in 3D: slab dynamics controlled mountain building and monsoon intensification. Lithosphere L636, 1. https://doi.org/10.1130/L636.1.
Wei, W., Xu, J., Zhao, D., Shi, Y., 2012. East Asia mantle tomography: new insight into plate subduction and intraplate volcanism. J. Asian Earth Sci. 60, 88–103. https://doi.org/10.1016/j.jseaes.2012.08.001.
Wessel, P., Luis, J.F., Uieda, L., Scharroo, R., Wobbe, F., Smith, W.H.F., Tian, D., 2019. The generic mapping tools version 6. Geochem. Geophys. Geosyst. 20. https://doi.org/10.1029/2019GC008515.
Wittlinger, G., Masson, F., Poupinet, G., Tapponnier, P., Mei, J., Herquel, G., Guilbert, J., Achauer, U., Guanqi, X., Danian, S., Lithoscope Kunlun Team, 1996. Seismic tomography of northern Tibet and Kunlun: evidence for crustal blocks and mantle velocity contrasts. Earth Planet. Sci. Lett. 139, 263–279. https://doi.org/10.1016/0012-821X(95)00235-5.
Xu, M., Huang, H., Huang, Z., Wang, P., Wang, L., Xu, M., Mi, N., Li, H., Yu, D., Yuan, X., 2018. Insight into the subducted Indian slab and origin of the Tengchong volcano in SE Tibet from receiver function analysis. Earth Planet. Sci. Lett. https://doi.org/10.1016/j.epsl.2017.11.048.
Yin, A., 2010. Cenozoic tectonic evolution of Asia: a preliminary synthesis. Tectonophysics 488, 293–325. https://doi.org/10.1016/j.tecto.2009.06.002.
Yin, A., Harrison, T.M., 2000. Geologic evolution of the Himalayan-Tibetan Orogen. Annu. Rev. Earth Planet. Sci. 28, 211–280. https://doi.org/10.1146/annurev.earth.28.1.211.
Yue, H., Chen, Y.J., Sandvol, E., Ni, J., Hearn, T., Zhou, S., Feng, Y., Ge, Z., Trujillo, A., Wang, Y., Jin, G., Jiang, M., Tang, Y., Liang, X., Wei, S., Wang, H., Fan, W., Liu, Z., 2012. Lithospheric and upper mantle structure of the northeastern Tibetan Plateau. Journal of Geophysical Research: Solid Earth 117, B5. https://doi.org/10.1029/2011JB008545.
Zhang, H., Zhao, J., Xu, Q., 2012. Crustal and upper mantle velocity structure beneath central Tibet by P-wave teleseismic tomography. Geophys. J. Int. 190, 1325–1334. https://doi.org/10.1111/j.1365-246X.2012.05582.x.
Zhang, H., Zhao, D., Zhao, J., Liu, H., 2015. Tomographic imaging of the underthrusting Indian slab and mantle upwelling beneath central Tibet. Gondwana Res. 28, 121–132. https://doi.org/10.1016/j.gr.2014.02.012.
Zhao, J., Yuan, X., Liu, H., Kumar, P., Pei, S., Kind, R., Zhang, Z., Teng, J., Ding, L., Gao, X., Xu, Q., Wang, W., 2010. The boundary between the Indian and Asian tectonic plates below Tibet. Proc. Natl. Acad. Sci. U. S. A. 107, 11229–11233. https://doi.org/10.1073/pnas.1001921107.